Penerbit Akademia Baru

Journal of Advanced Research in Fluid Mechanics and Thermal Sciences

Journal homepage: www.akademiabaru.com/arfmts.html
ISSN: 2289-7879

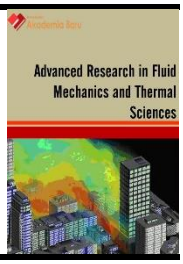

Numerical Study of Upward Vertical Two-Phase Flow Through an Annulus Concentric Pipe

Open Access

Hamza Gouidmi [1,2,*], Razik Benderradji [2,3], Abdelhadi Beghidja [2], Tahar Tayebi [1,4]

[1] Faculty of Sciences and Technology, Mohamed El Bachir El Ibrahimi University, Bordj Bou Arreridj, El-Anasser 34295, Algeria
[2] Laboratory of Renewable Energies and Sustainable Development, Faculty of technology sciences, Mentouri Brothers Constantine 1 University, Constantine 16261, Algeria
[3] Faculty of Science Mohamed Boudiaf University, M'Sila- Algeria
[4] Energy Physics Laboratory, Department of Physics, Faculty of Science, Mentouri Brothers Constantine 1 University, Constantine 16261, Algeria

ARTICLE INFO

Article history:
Received 20 February 2019
Received in revised form 24 March 2019
Accepted 21 May 2019
Available online 16 June 2019

Keywords:
Two-phase flow pattern; VOF model (volume of fluid); volume fractions; concentric annulus

ABSTRACT

This study provides a 3D numerical simulation of two-phase flow in upward vertical annuli pipe using the Fluent CFD commercial code. The condition of two-phase flow was simulated with the Volume of Fluid (VOF) model, taking into consideration turbulence effects using the k-e model. The internal and external diameters of the pipe are D_T=12.7 mm, D_C=38.1 mm, respectively and length L=16 m. Numerical results were obtained for various values of air velocity, Ug at fixed water velocity (U_l =0.14 m/s). In this numerical simulation, we have identified global flux structures and their transition regimes, such as the size and shape of bubbles, slug and their zigzag and coalescence phenomena. These flow regimes have been clearly influenced by the air velocity. The results obtained have been validated and are consistent with those experimentally reported.

1. Introduction

Two-phase water-air and liquid-vapor flows are found in industrial systems, such as the transport of natural gas and oil, thermal power stations (conventional or nuclear), etc. Several problems have been encountered in these industrial systems and have remained to be solved. The lacks of the analyzes and the numerical simulations of these industrial systems, related to performance and/or safety problems, require more and more a better physical knowledge of the local characteristics of the flows. The Volume of Fluid (VOF) approach of the two-fluid model allows a detailed description of the two-phase flows due to the writing of mass balances, momentum for each phase. The terms of interfacial transfers appearing during the establishment of the averaged equations of the model gather all the characteristics of the interactions between the two phases. This is why the transition phenomena between liquid-gas, adiabatic, non-reactive two-phase flow pattern in simple geometries

* *Corresponding author.*
E-mail address: gouidmi@yahoo.fr (Hamza Gouidmi)

or characteristic multidimensional configurations are the subject of numerous studies, in particular the geometries of the annulus pipes. There are recent published works on upward vertical pipe flow regimes suggesting the presence of five basic flow patterns: bubble, dispersed bubble, liquids plug or gas slug, churn and annular.

These experimental works reveal that, although the same flow regimes occur an annulus pipes, their characteristics may be substantially different. Two geometrical parameters identify these flow patterns: the diameter ratio of the annulus pipe K= (D_T/D_C) and the degree of eccentricity e=(2DBC/(D_C-D_T)); where DBC is the distance between the centers of the two pipes. The annuli may have eccentricity values ranging from zero to one. Figure 1 (Caetano *et al.,* [1]) shows the cross sections of the annuli with the same value of pipe diameter ratio, K, and for eccentricities of 0.0, 0.5 and 1.0. Therefore; the two-phase flow patterns in annulus pipes are presented in Figure 2(a) and 2(b) plotted by Caetano *et al.,* [1]. Several experimental of [1-10], theoretical [11-13] and analytical studies [12-20] are performed on two-phase gas/liquid, vapor/liquid upward or downward flows in the annulus pipes in the case where the absence of heat transfer by the wall of the pipe to identify their overall structures and their flow pattern. However, in the case of a presence the heat exchange in the annular pipe, we quote some articles, such as, the works of [21-22].

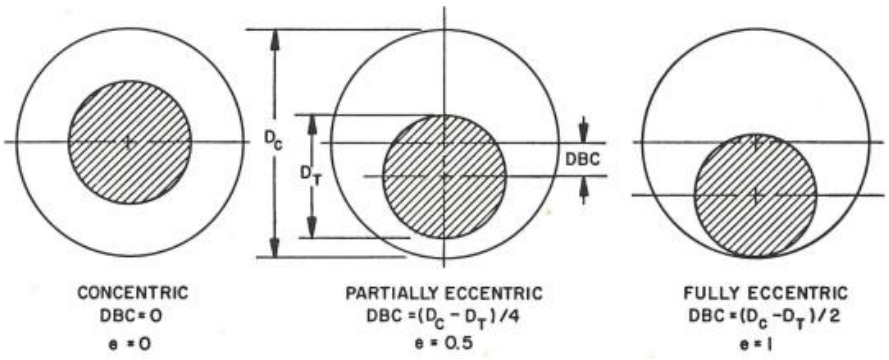

Fig. 1. Annuli configuration

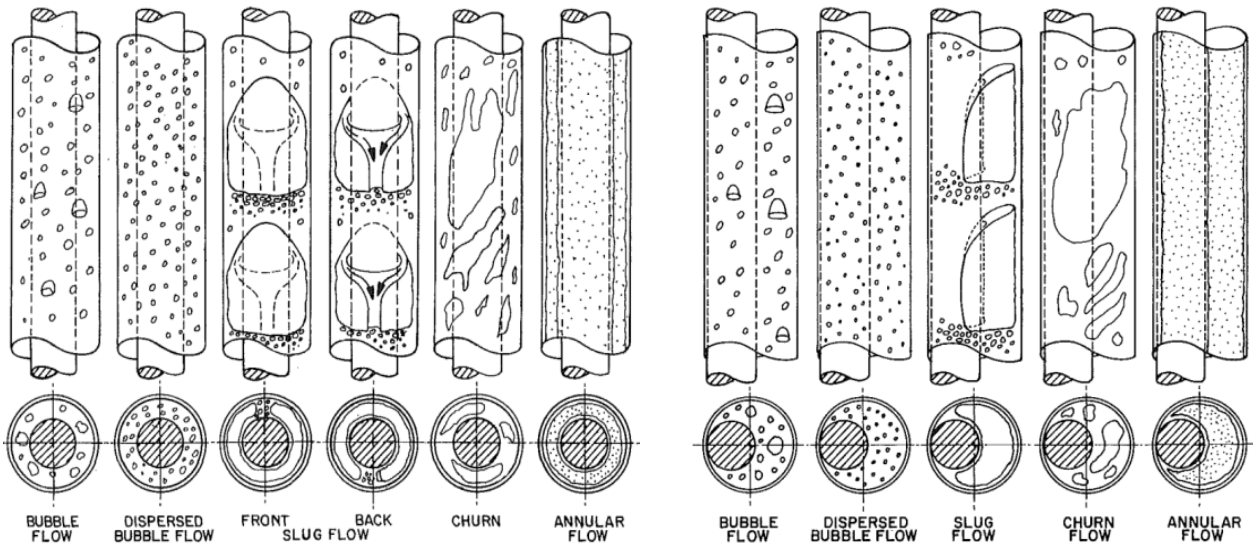

Fig. 2. Flow patterns in upward vertical flow through (a) a concentric, (b) a fully eccentric annulus pipe [1]

Many studies have been devoted to this type of flow. Consequently, in concentric annulus pipe configurations, we carry out a numerical study capable of providing some physical details of the influence of the air inlet velocity where the water velocity remains constant in all calculations equal

to 0.14 m/s. The ability to take into account the phenomena thus observed by experiments and models conventionally encountered in the literature could also be analyzed by means of the Fluent commercial code.

2. Methodology

2.1 Descriptions of the Configuration and Numerical Method

We carry out our study based on the experimental studies of Das *et al.,* [3] by using the same configuration. it is a vertical pipe of an annular transverse section of length L = 16m and internal and external diameter equal to 12.7mm and 38.1mm, respectively, as presented in Figure 3.

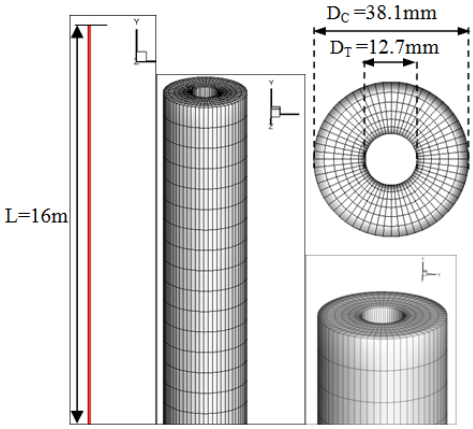

Fig. 3. Mesh and geometry of the computation domain

2.2 Governing Equations

Majority previous works, the movement of two-phase flow is performed in cases where the thermal exchanges have been neglected (the energy equation is negligible). This supposition was simulated with the Volume of Fluid (VOF) model, originally presented by Hirt and Nichols [23] on the basis of the Eulerian-Eulerian approach. In addition, the Fluent code [24] used a high-resolution interface capture scheme (HRIC) based on the compressive interface capture scheme for arbitrary meshes introduced by Ubbink [25] and improved by Peric and Muzaferija [26]. The geo-reconstruction scheme was used [24]. In the VOF method, the all variables fields and the properties are shared by the phases and represent the values averaged in volume, provided that the volume fraction of each of the phases is known at each position. Therefore, a single set of equations is solved across the flow domain, which depends on the volume fractions of all phases across properties ρ and μ. For a two-phase system, ρ and μ are related to the volume fraction by the following relationships.

$$\rho = \alpha\rho_1 + (1-\alpha)\,\rho_2 \quad \text{and} \quad \mu = \alpha\,\mu_1 + (1-\alpha)\,\mu_2 \tag{1}$$

The continuity equation, Eq. (2), provides a mass balance in the flow domain. The system of Eq. (3) describe the equation of motion which represents the balance of forces acting on the system. Once the Reynolds approach to turbulence modeling is applied, theses equations can be written in the form of Cartesian tensor as follows.

$$\frac{\partial \rho}{\partial t} + \frac{\partial(\rho u_j)}{\partial x_j} = 0 \tag{2}$$

$$\frac{\partial}{\partial t}(\rho u_i) + \frac{\partial}{\partial x_j}(\rho u_i u_j) = \frac{\partial p}{\partial x_i} + \frac{\partial p}{\partial x_j}\left[\mu_{eff}\left(\frac{\partial u_i}{\partial x_j} + \frac{\partial u_j}{\partial x_i} - \frac{2}{3}\delta_{ij}\frac{\partial u_i}{\partial x_i}\right)\right] + \frac{\partial}{\partial x_j}\left(-\rho\overline{u_i' u_j'}\right)_i \quad (3)$$

where u_i is the component i of the fluid velocity u, x_j is the spatial coordinate j, P is the static pressure, μ_{eff} is the effective viscosity, δ_{ij} is the Kronecker delta and $(-\rho\overline{u_i' u_j'})$ is the Reynolds stress. The monitoring of the interface (s) between the phases is carried out by the solution of a continuity equation for the volume fraction (α) of one (or more) of the phases.

The volume fraction field will have the following values: α=0 if the cell is empty, α = 1 if the cell is full, 0 <α <1 if the cell contains the interface between the two fluids. For the q^{th} phase, this equation has the following form

$$\frac{\partial \alpha_k}{\partial t} + \frac{\partial(\alpha_k u_j)}{\partial x_j} = \frac{S\alpha_k}{\rho_k} \quad (4)$$

where S is a source; the equation of the volume fraction will not be solved for the primary phase; the volume fraction of the primary phase will be calculated according to the condition

$$\sum_{k=1}^{n} \alpha_k = 1 \quad (5)$$

The surface tension at an interface between two fluids is the result of an imbalance of the attraction forces between the molecules at the interface between two fluids. In the VOF model, the surface tension is introduced as a body force acting on the grid cells that contain the interface by adding a pulse source term to the momentum equation. In Fluent, the surface tension model is the CSF (Continuum Surface Force) model proposed by Brackbill *et al.,* [27]. The pressure drop across the surface depends on the value of the surface tension. The fact that the two fluids are supposed to share the same equations of momentum limits the relevance of the VOF method for cases where the velocity difference between the two fluids is important. The solution to all the equations was obtained using the Fluent commercial code. For calculating the flows at the control volume interfaces required by the VOF model, a second order discretization scheme was used. It is important to take into account the turbulence of the numerical simulation because it is obvious that even in the case of low flow rates, the Taylor bubbles that rise through the liquid create a film developing around themselves and a wake in the tail. A high velocity gradient should occur at the gas-liquid interface, with the gas phase moving much faster than the liquid phase. In order to simulate turbulence, the standard model of k-ε, Launder and Spalding [28], which requires the flow to be completely turbulent, has been used for several reasons; the model is computationally efficient, is implemented in many commercial codes, the pipe geometry is not complicated and has demonstrated its ability to correctly simulate many industrial processes, including multi-phase flow. Shen *et al.,* [29] applied the k-ε model with VOF. The model is described by the following elliptic equations needed to close the averaged Reynolds Navier Stokes equations (RANS).

$$\frac{\partial}{\partial t}(\bar{\rho}k) + \frac{\partial}{\partial x_j}(\bar{\rho}\tilde{u}_j k) = \frac{\partial}{\partial x_j}\left[\left(\bar{\mu} + \frac{\overline{\mu_t}}{Pr_k}\right)\frac{\partial k}{\partial x_j}\right] + G_k + G_b - \bar{\rho}\varepsilon - Y_M + S_k \quad (6)$$

$$\frac{\partial}{\partial t}(\bar{\rho}\varepsilon) + \frac{\partial}{\partial x_j}(\bar{\rho}\tilde{u}_j \varepsilon) = \frac{\partial}{\partial x_j}\left[\left(\bar{\mu} + \frac{\overline{\mu_t}}{Pr_\varepsilon}\right)\frac{\partial \varepsilon}{\partial x_j}\right] + C_{\varepsilon 1}\frac{\bar{\rho}\varepsilon}{k}(G_k + C_{\varepsilon 3}G_b) - C_{\varepsilon 2}\frac{\bar{\rho}\varepsilon^2}{k} + S_\varepsilon \quad (7)$$

In the equations given above, k is the turbulent kinetic energy; ε is the dissipation rate of k. σ_k, σ_ε, C_1 and C_2 are constants whose values are 1.0, 1.3, 1.44 and 1.92 respectively, u_i is the component i

of the fluid velocity u, x_j is the spatial coordinate j. The viscosity of the fluid should be corrected for turbulence in the Navier-Stokes equations using an effective viscosity $\mu_{eff}=\mu+\mu_t$ where μ is the dynamic viscosity and μ_t is the turbulent viscosity.

2.3 Initials and Boundary Conditions

Once the mesh is generated, the computation domain boundaries are specified. The boundary type specifications define the physical and operational characteristics of the model at the level of the topological features that represent the model's boundaries. At the walls, conditions were assumed to be non-slip, and the approach of the wall function is used. The non-slip condition (v=0) is the appropriate condition for the velocity component on the solid walls, since the fluid in contact with the wall is stationary. At the entrance, velocities for both phases were referred to as superficial velocities. The phases have been clearly defined with the primary phase as water and the secondary phase as air. The volume fraction and the density of each phase were both prescribed at the entrance. The summary of the boundary conditions specifications is as follows.

At the Inlet → velocity inlet
At the outlet → pressure outlet
At the Wall → no slip condition

The domain initially was represented as full of liquid phase, except, it remains certain small distance is repacked by atmospheric air with velocities fields equal to zero.

2.4 Algorithm of Solution

In order to solve numerically the system of partial differential equations, the discretization of the equations was performed using the Fluent solver which is based on the finite volume method (FVM). Since Fluent uses a separate solver for VOF, the discretization scheme of their parameters is explicit; the continuity and momentum equations must be related. Various techniques are reported in the literature. However, the PISO (Pressure implicit with Splinting of Operators) algorithm, which stands for implicit method for pressure equations, Patankar and Spalding [30], is applied to control the overall solution because of its good performance to find a convergent solution quickly. In addition, the iterative solver was significantly accelerated using an Algebraic Multigrid (AMG) technique to obtain a better convergence rate. Relaxation factors of 0.3, 0.7, and 0.8, respectively, were applied to the pressure, moment, and turbulent kinetic energy parameters as recommended by Fluent.

2.5 Two-phase Flow Parameters at the Input

The two-phase flow parameters (air and water) are presented in the Table 1. They are defined by the two phase's velocities. These parameters are chosen from the map of Das *et al.,* [1], there followed the two-phase flow pattern encountered.

Table 1
Two-phase flow parameters

Air velocity	Water velocity
0.05	0.14
0.1	0.14
0.123	0.14
0.244	0.14
0.37	0.14
0.955	0.14
2.11	0.14
5	0.14
12	0.14

2.6 Effect of Mesh

The 3D mesh selected is quadrilateral structured and refined close to the surface of the inner tube. Before doing the calculation, we checked and confirmed which mesh is chosen. The mesh chosen is dependent on the accuracy and calculation time. Three different meshes are considered as indicated below in Table 2.

Table 2
Presentation of the three mesh

Mesh type	Cells number
M 1	292314 Cells
M 2	647260 Cells
M 3	1263732 Cells

Our simulations are performed at a constant liquid velocity, U_l =0.14 m/s, and for different air velocity as indicated on the Table 1 above. The mesh effect is presented in Figure 4 taking the superficial velocity of the first bubble as a function of time at an air and water velocities equal to 5m/s and 0.14m/s, respectively. This figure shows that the evolution of the velocity with time is almost constant for the three meshes. In addition, the two meshes M2 and M1 having close results. Therefore, we can select the M2 Mesh which has 647260 cells corresponding 687479 nodes.

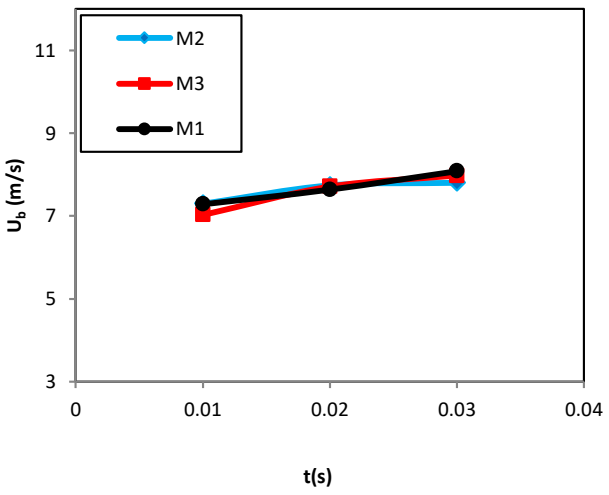

Fig. 4. Presentation of the mesh effect, carried out for U_g = 5m /s and U_l = 0.14m /s

2.7 Validation

In order to give more confidence of our results performed by the three-dimensional numerical simulation, we compared them with those obtained by the experiment of Das *et al.,* [6]. It is found that the volume fractions air by the numerical computations (see Figure 5) almost give clear and legible conformity with the drawn regimes by Das *et al.,* [6]. The comparison outcomes appear to establish the validity and accuracy of our numerical approach.

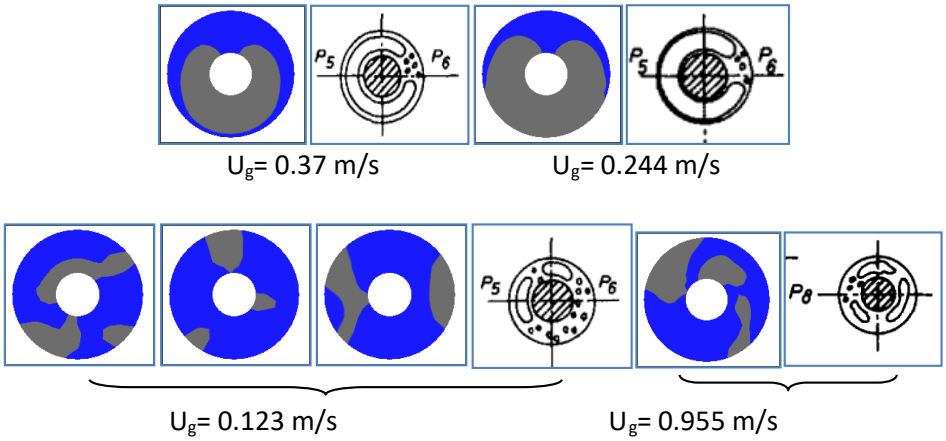

Fig. 5. Validation of our results, three flow patterns comparison: (a) bubble regime, (b) Slug regime and (c) high coalescence regime of our results presented by the volume fraction and the diagrams of the work of Das *et al.,* are carried out for U_l = 0.14m/s

3. Results and Discussion

3.1 Flow Patterns Observed

Before giving a detail for the results of the numerical calculation, we can present the flow regimes observed, as follows.

3.1.1 Bubble flow

This flow pattern is characterized by a discontinuous gaseous (air) phase that is distributed as discrete bubbles rising through a continuous liquid (water) phase. These discrete air bubbles tend to have a spherical shape and exhibit slippage through the liquid phase due to buoyancy forces. The bubble flow profile occurs at low superficial velocities air at low average liquid velocities. This regime is carried out under two-phase flow conditions where the air velocity is equal to 0.05 m/s and for a water velocity equal to 0.14 m/s. Figure 6 shows the iso-surfaces colored by the air volume fraction. It is observed that the first large bubble noted Taylor's bubble is glued and surrounded on the surface of the internal tube and some small air bubbles below and back thereof have different sizes and are dispersed in the continuous liquid phase. The size of it (much smaller than the pipe diameter), the shape (usually spherical or elongated) and the bubble density distribution (uniform, peak or peak) depends on the geometry and the inclination pipe relative to the vertical.

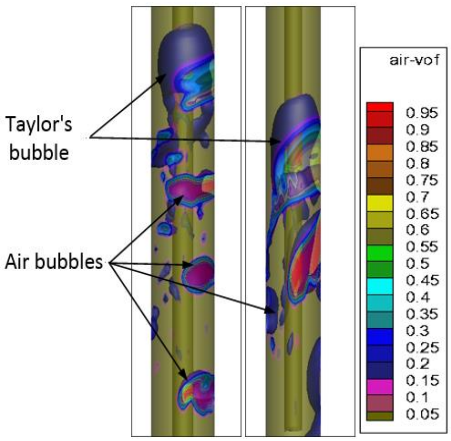

a) t= 1.8s b) t= 1.04s

Fig. 6. Iso-surfaces of the Q criterion at two different time steps colored by the air volume fractions presented the bubbles régime for U_l=0.14 m / s and: a) U_g =0.05 m/s, b) U_g =0.1m/s

3.1.2 Slug flow

The slug flow occurs over a wide range of flow rates and is one of the most frequently encountered flow regimes in two-phase flows. It is characterized by the alternating flow of air and liquid. The gaseous phase (air) appears in two different forms: large and small spherical bubbles dispersed in the water phase. Large bubbles occupy almost the entire cross section of the annular surface and move uniformly upwards. The liquid phase (of water) appears both in the form of liquid plugs which bridge the cross section of the annular pipe and in the form of falling liquid films which flow downwards between the large bubbles (slugs air) and the walls of the tubes, see Figure 7(d). The slugs (water) which separate the main successive bubbles contain small dispersed spherical gas (air) bubbles. The complex distribution of the two phases and the nature of the intermittent regime make the slug flow difficult to modeling.

Figure 7(a)-(d), show the iso-surfaces colored by the volume fraction of air, which are carried out under two-phase flow conditions where the velocity of the gas takes the values (0.244 and 0, 37) m/s and the water velocity equal to 0.14 m/s, kept constant. It is observed that the regime detected in this figure is the slug regime. We also observe that, the shape of these big bubbles is nonsymmetrical relative to the axis of the annulus, it comprises two faces, one frontal and the other back opposite thereof face. The first face occupies almost all the annular space, while the second has an open cavity towards the center of the annulus. The circulating liquid (water) contained in the cavity is directed in the opposite direction to the main flow.

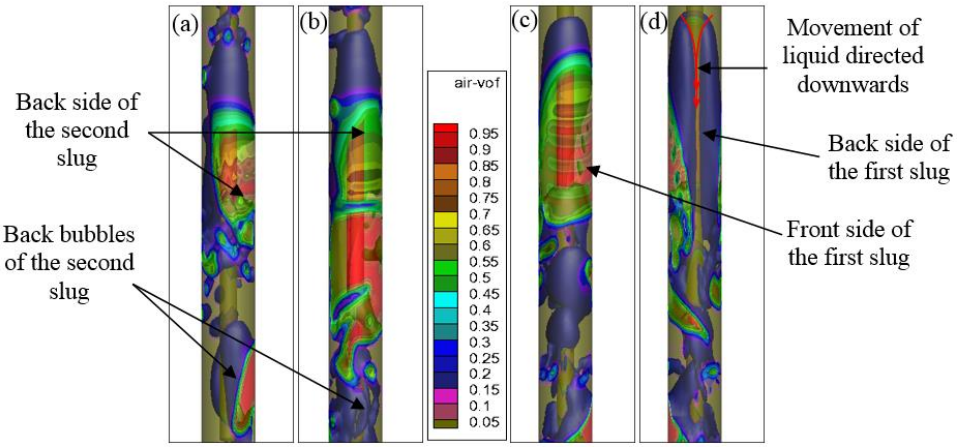

Fig. 7. Iso-surfaces of the Q criterion at two different time steps colored by the volume fractions of air presented the bubbles régime for U_l=0.1m/s

3.1.3 The regime with strong coalescence (Churn flow)

This flow pattern may be similar to the slug flow. However, it is much more chaotic, sparkling and messy. Taylor's bubble becomes small and its shape is deformed. The liquid (water) between the successive Taylor bubbles is also deformed at several sites by the air flowing at a high velocity; see the Figure 8(a), so the void fraction of air is important. In this type of flow pattern, the air slugs will become more and more elongated. As it happens, the liquid (water) in the slug falls back, accumulates forms a temporary bridge and is again lifted up by the air. This alternate direction for the movement of the liquid (water) is a typical feature of strong coalescence.

3.1.4 The annular flow

An annular flow occurs at high superficial gas velocities and is characterized by a fast-moving, continuous gas phase (air) flowing through the core of the ring cross section shown in the Figure 8(b). The liquid phase (water) elapses both in the form of liquid films wetting the walls of the tubes and in the form of small droplets of water entrained in the gaseous nucleus (air). The outer film, which wets the wall of the outer tube, is usually thicker than the inner film which elapses on the outer wall of the inner tube. The droplets of air and water circulating in the core can be considered as a homogeneous mixture due to the high velocity of the gas phase (air).

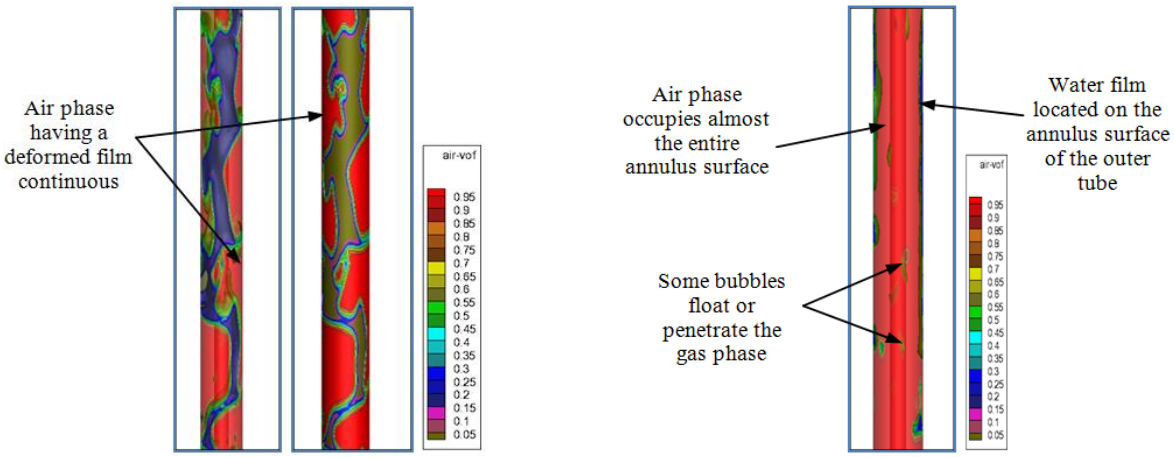

(a) U_g =5m/s at t=4.4s (b) U_g =12m/s at t=2.9s

Fig. 8. Iso-surfaces of the Q criterion colored by the volume fractions of air presented the Churn régime (in the left) and the annular régime (in the right) for U_l=0.14 m/s

3.2 Flow Pattern Transition

The transition patterns are characterized by alternating appearance of bubbles and slug of gas. The major difference between elongated bubble flow and slug flow is that the first does not contain gas bubbles entrained in the liquid slug.

3.2.1 Transition from bubbly to slug flow

Then, numerical simulations were made for a fixed water flow (corresponds to a liquid velocity U_l=0.14m/s) by varying the air flow rate until the transition criteria between the flow of the bubble and that of the plug are satisfied. The flow velocities of the air and water at which the bubble flow profile changes to pocket flow are plotted in Figure 10 of the flow map of Das *et al.,* [3].

Then, the air flow is changed to step and the same procedures are followed to obtain the point following the map of considered flow pattern. If the coalescence is favored, larger bubbles form and move towards the center of the annulus, showing the tip pattern of the nucleus before the slug flow pattern. Another clue that justifies the transition from the bubbles flow to slug flow is the density of the small bubbles, which lies between the big bubbles of Taylor, whether it is increasing or important.

For a comparison of the bubbles to slug transition limit estimated by the numerical calculation, where U_g = (0.123 and 0.1) m/s, with the available experimental results observed by the map of Das *et al.,* is shown in Figure 9(a). It can be seen from this figure that the numerical results correspond well to experimental observation.

3.2.2 Transition from slug to Churn flow

The second transition from slug to churn flow is calculated for U_g = 2.11 m/s is shown in Figure 9(b). It is found that the length slug is longer than that of the first transition. This remark is translated by the position of the point corresponding to this velocity on the map of Das *et al.,* [3] of Figure 10.

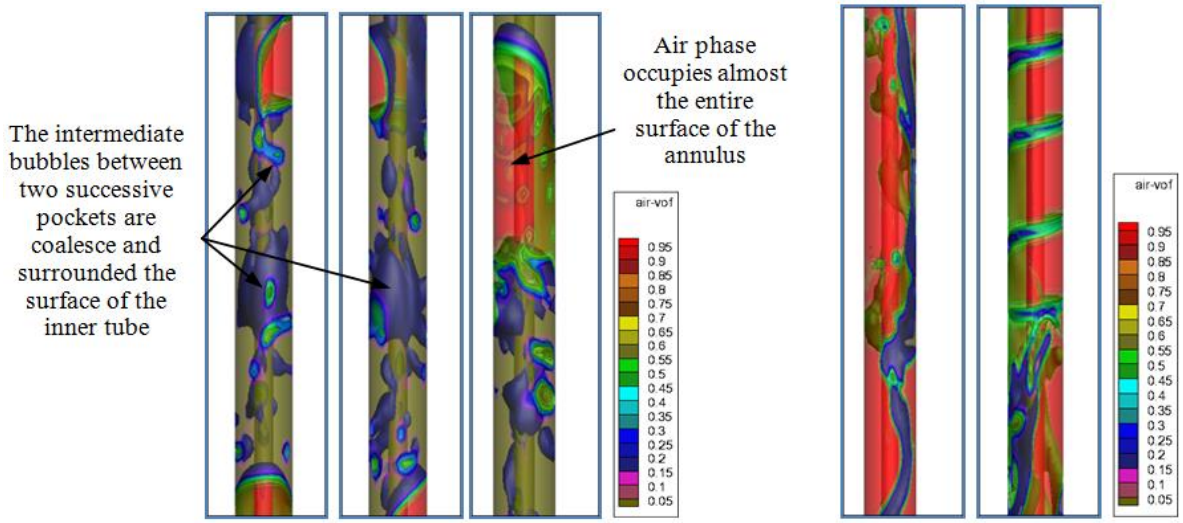

(a) U_g = 0.123m/s at t= 3.85s (b) U_g =2.11m/s

Fig. 9. Iso-surfaces of the Q criterion at colored by the volume fractions of air presented the transition from bubbles regime to slug régime (left) and the transition from slug regime to Churn régime (right) for U_l = 0.14 m/s

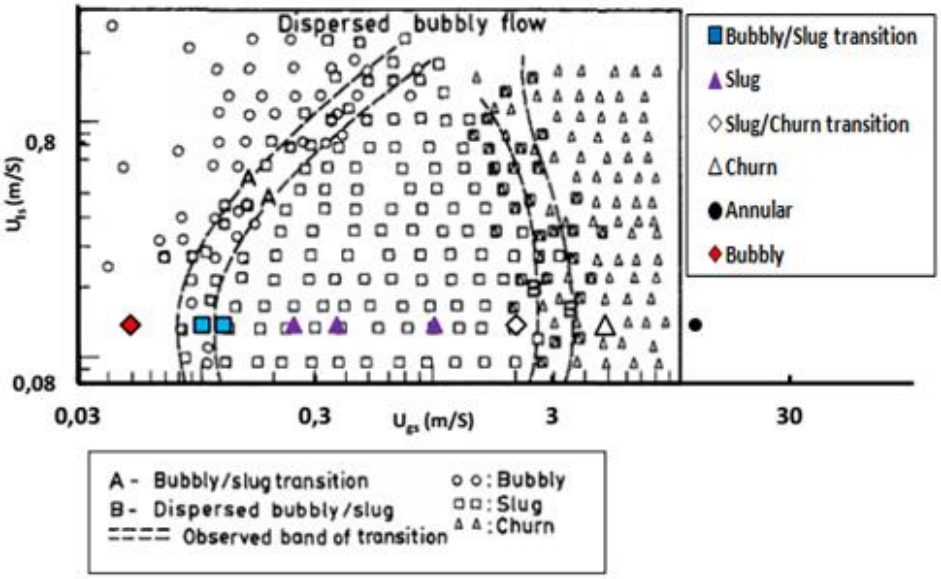

Fig. 10. Points of selected velocity plotted on the water-to-air flow chart of Das *et al.,* [3]

3.3 Effect of Air Velocity on the Physical Processes Encountered

3.3.1 Coalescence process

Several processes that were observed by the researchers before and observed during this study, mention two, the process of coalescence of the bubbles or the slug, the zigzag of the bubbles. Regarding the coalescence process, it is observed in all cases of air velocity either for bubbles or for slug see Figure 11 and 12, respectively. In both cases this process is managed by increasing the slug size of bubbles as a function of time and during the displacement of these.

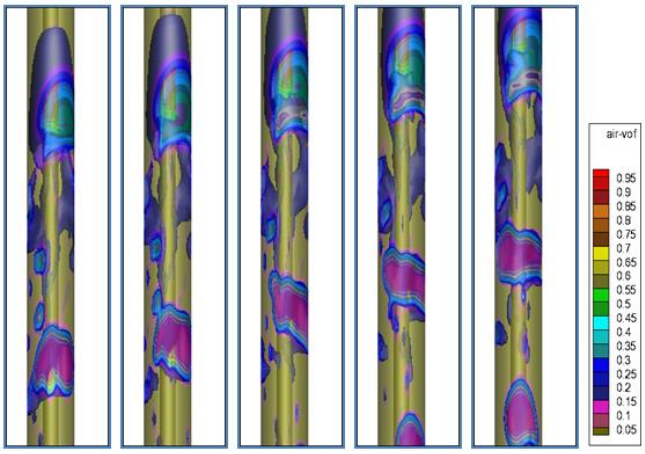

t= 1.69s 1.71s 1.74s 1.7s 1.8s

Fig. 11. Isosurfaces of the Q criterion at different time steps colored by the volume fractions of air presented the coalescence processes for U_l = 0.14 m/s and U_g =0.05m/s

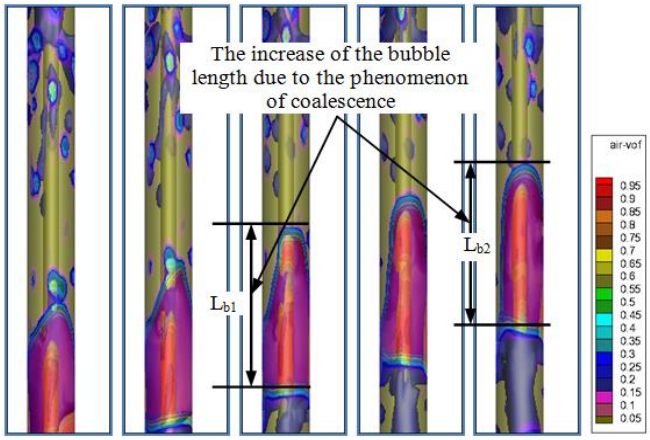

t= 3.73s 3.76s 3.79s 3.82s 3.85s

Fig. 12. Isosurfaces of the Q criterion at different time steps colored by the volume fractions of air presented the coalescence processes for U_l=0.14 m/s and U_g =0.1m/s

3.3.2 Zigzag process

While the zigzag process was usually captured only in the bubbles rarely observed in the slugs. These two processes are presented for an air velocity U_g = (0.05, 0.123 and 0.37) m/s, we present only two cases in Figure 13 and 14 superposed and followed with two-phase flow pattern.

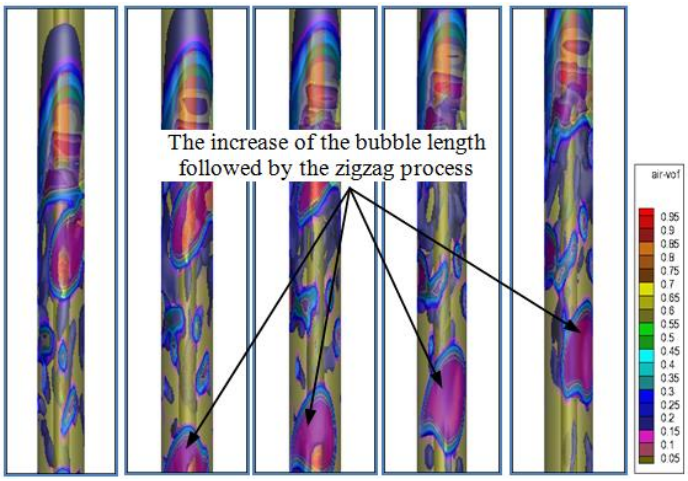

Fig. 13. Isosurfaces of the Q criterion at different time steps colored by the volume fractions of air presented the zigzaq processes for U_l=0.14 m/s and U_g =0.1m/s

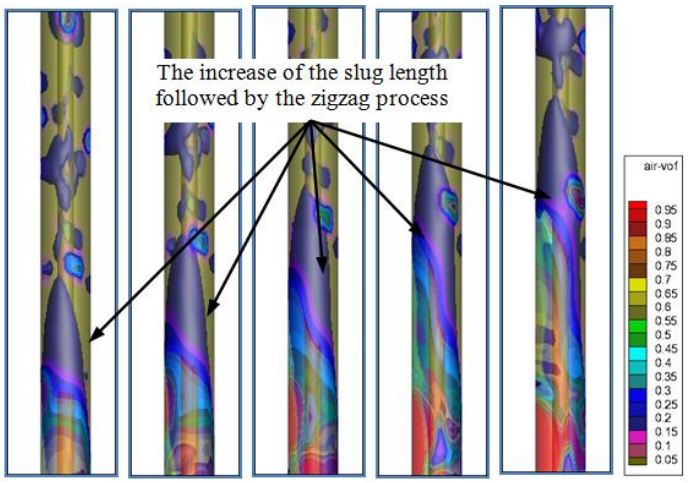

Fig. 14. Isosurfaces of the Q criterion at different time steps colored by the volume fractions of air presented the zigzaq processes for U_l=0.14 m/s and U_g =0.37m/s

3.4 Effect of Air Velocity on Flow Behavior in Vertical Cross Symmetry Planes

We can identify in the following presentations the different two-phase flow regimes at the vertical cross-symmetry planes (x = 0 and z = 0) by successive temporal air volume fraction fields recorded during simulation with a time step Δt = 0.03s.

3.4.1 Bubble flow

Figure 15 (in the left), represents the contours of the volume fraction of the air at U_g = 0.05 m/s for U_l=0.14m/s at two successive times t = 1.69s and 1.71s. A complete cut of the early Taylor's bubble is observed on the x = 0 plane, while it is displayed by a half-section and is followed by small dispersed bubbles in the annular space on the z = 0 plane. These intermediate Taylor bubbles have low density

in this space. These remarks indicate no complete occupation of the Taylor's bubble of the annulus, there they explaining the bubble regime.

3.4.2 Slug flow

This regime is observed in Figure 15 (in the right) for an air velocity U_g= 0.244m/s and U_l= 0.14m/s at two successive times. In this figure, the cut of the beginning pockets appear are uniform and symmetrical relative to the inner tube on the x = 0 plane. While they appear their halves on the plane z = 0. The elongated Taylor bubbles (the slugs) have large sizes. This is explained by the coalescence phenomenon. As air velocity increases, these slugs will become unstable shapes.

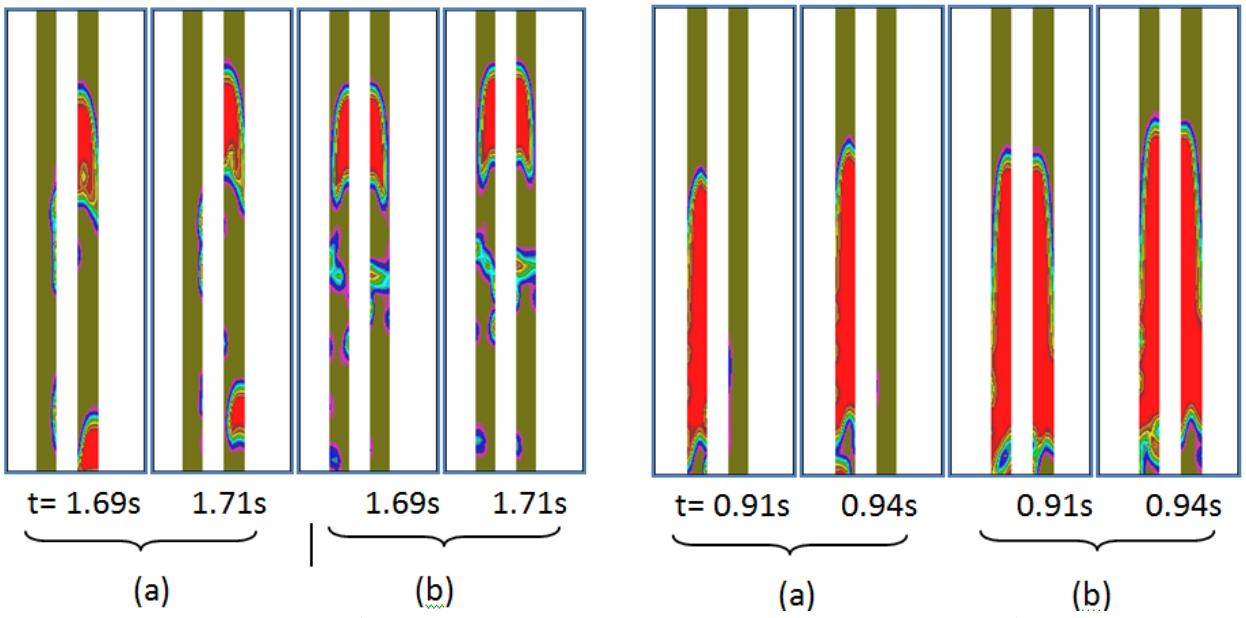

Fig. 15. Evolution of the volume fractions of the temporal air at and U_l = 0.14 m/s: in the symmetry planes ((a) z = 0, (b) x = 0)

3.5 Fields and Cross-sectional Distributions of Local Volume Fractions and Mixture Total Velocity Vectors

3.5.1 On the plans (xoz) and on the axes ox and oz

The qualitative visualization of the transverse distribution of the local volume fractions and the mixture total velocity vectors followed by their fields gives a better understanding of the quality of the predictions. In Figure 16 (left, right and bottom) presents the fields of the air volume fraction and the mixture total velocity vectors for different heights on the horizontal plane (xoz). The purpose of this presentation is to follow the development of two-phase flow pattern (bubble, slug, strongly coalesced or agitated).

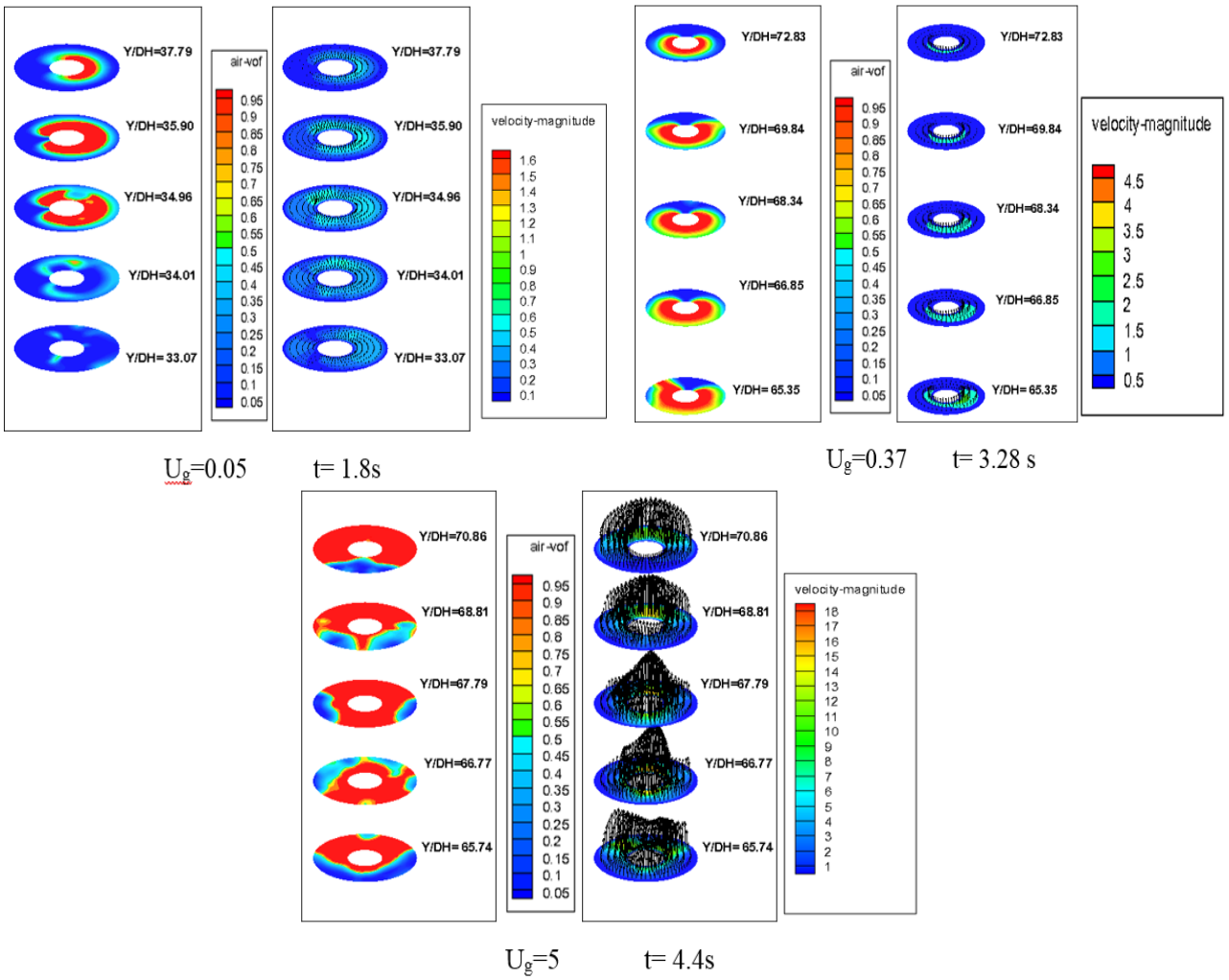

Fig. 16. Transverse contours of the volume fraction averaged of air over time (left) and velocity fields (right) for different vertical positions and for different air velocity

Figure 17, 18 and 19 represent the mixture total velocity profiles and the volume fraction of air on oriented lines following the ox and oz axes for different times. Knowing that, each profile corresponds to a well specified regime.

In the first place, Figure 17, represents the bubbles regime which corresponds to an air velocity U_g=0.05 m/s and a water velocity U_l= 0.14m/s. It can be seen that the evolutions of the air volume fractions are different according to their projection plans. The evolutions of these fractions in the planes from bottom to top are marked with zero values close to the external surface of the inner tube; this can be said that no bubbles located at the level of this surface. They are marked close to the inner surface of the outer tube, but with a weak presence, are with a rate not exceeding 5%. For evolutions in the lines of the high planes, one notices that the air volume fractions evolution increases when one arrives at a symmetrical evolution for one of the axes (at x = 0). For the other axis the evolutions remain zero. Whereas, for the mixture velocity profiles evolutions, a normal evolution of the velocity profile in this annular tube is observed, it is the same as that observed in a circular tube.

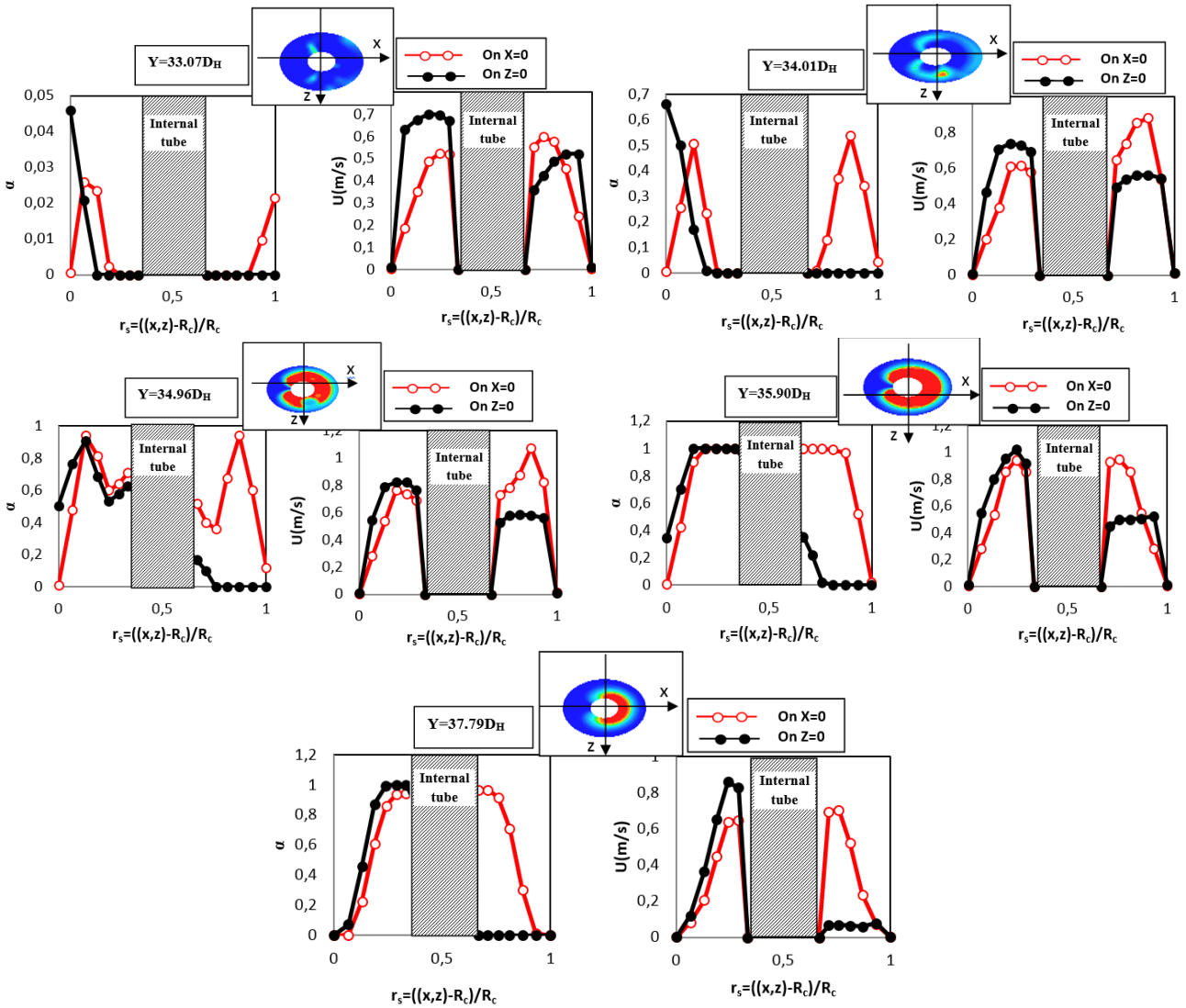

Fig. 17. Evolutions of Air volume fractions (left), and mixture total velocity (right) at different heights: 33.07D_H, 34.01D_H, 34.96D_H, 35.90D_H, y=37.79D_H, for U_g= 0.05 m/s

In second place in Figure 18, for the slug regime, which corresponds to an air velocity U_g= 0.37 m/s. It is found that the air volume fraction evolutions one of the lines oriented towards the axis (x=0), are null almost for all the planes. Whereas for the other glued lines on the oz axis, the evolutions are almost symmetrical relative to the center of the inner tube. This remark is explained by the surrounding of the slug of air on the outer surface of the inner tube. And for the mixture velocity profiles, we notice peaks, which translate by the displacement of certain bubbles to the outer surface of the inner tube.

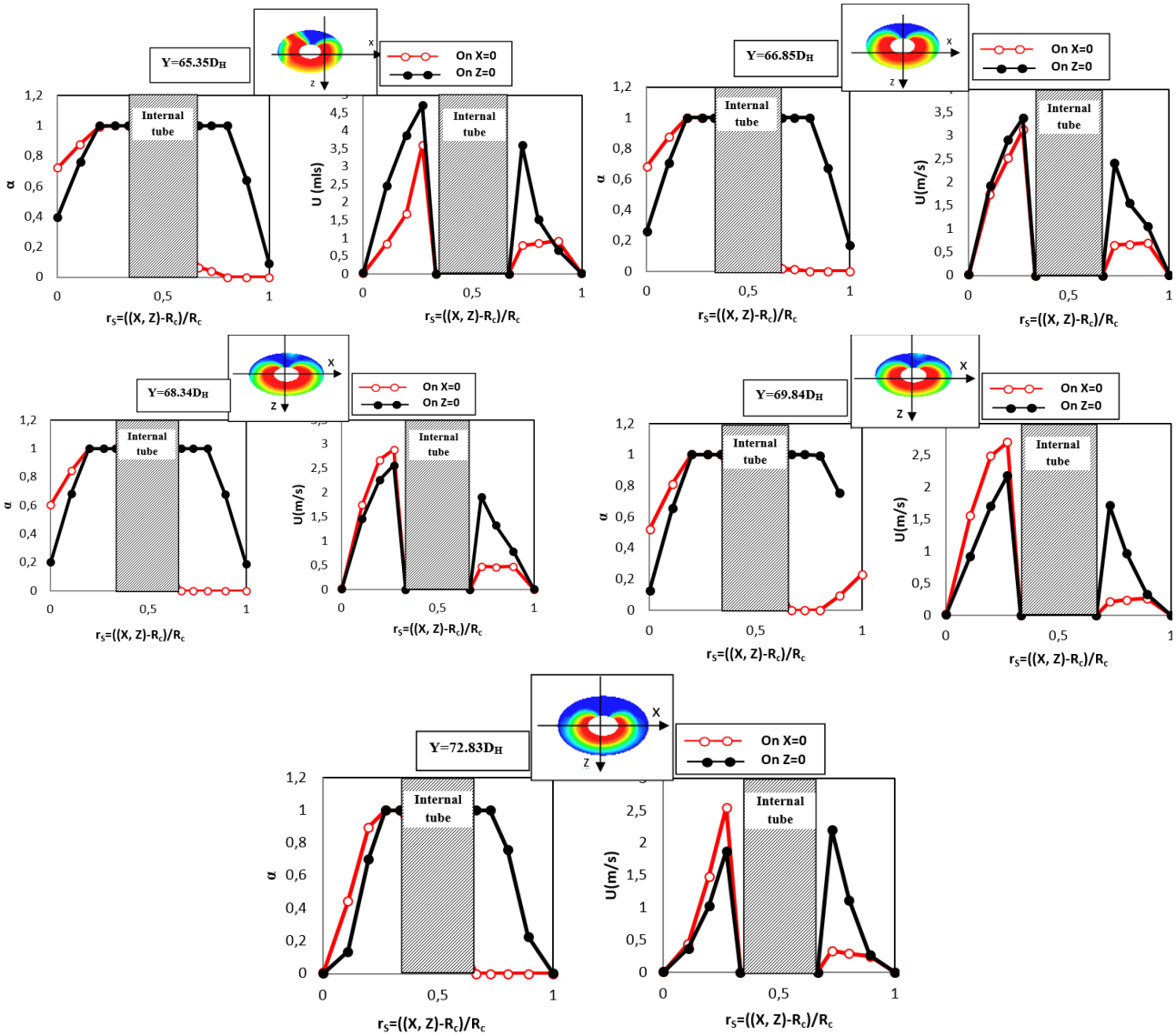

Fig. 18. Evolutions of Air volume fractions (left), and mixture total velocity (right) at different heights: y=65.35D_H, 66.85D_H, 68.34D_H, 69.84D_H, 72.83D_H for U_g = 0.37 m/s

In third place in Figure 19, for the regime with strong coalescence, which corresponds to an air velocity U_g= 5 m/s. It is noted that the air volume fractions evolutions are important for all the planes, they explain by the occupation of the air in the majority of the annular space. While, the mixture velocity evolutions, take the same evolutions as the preceding cases, but with an increase of their values.

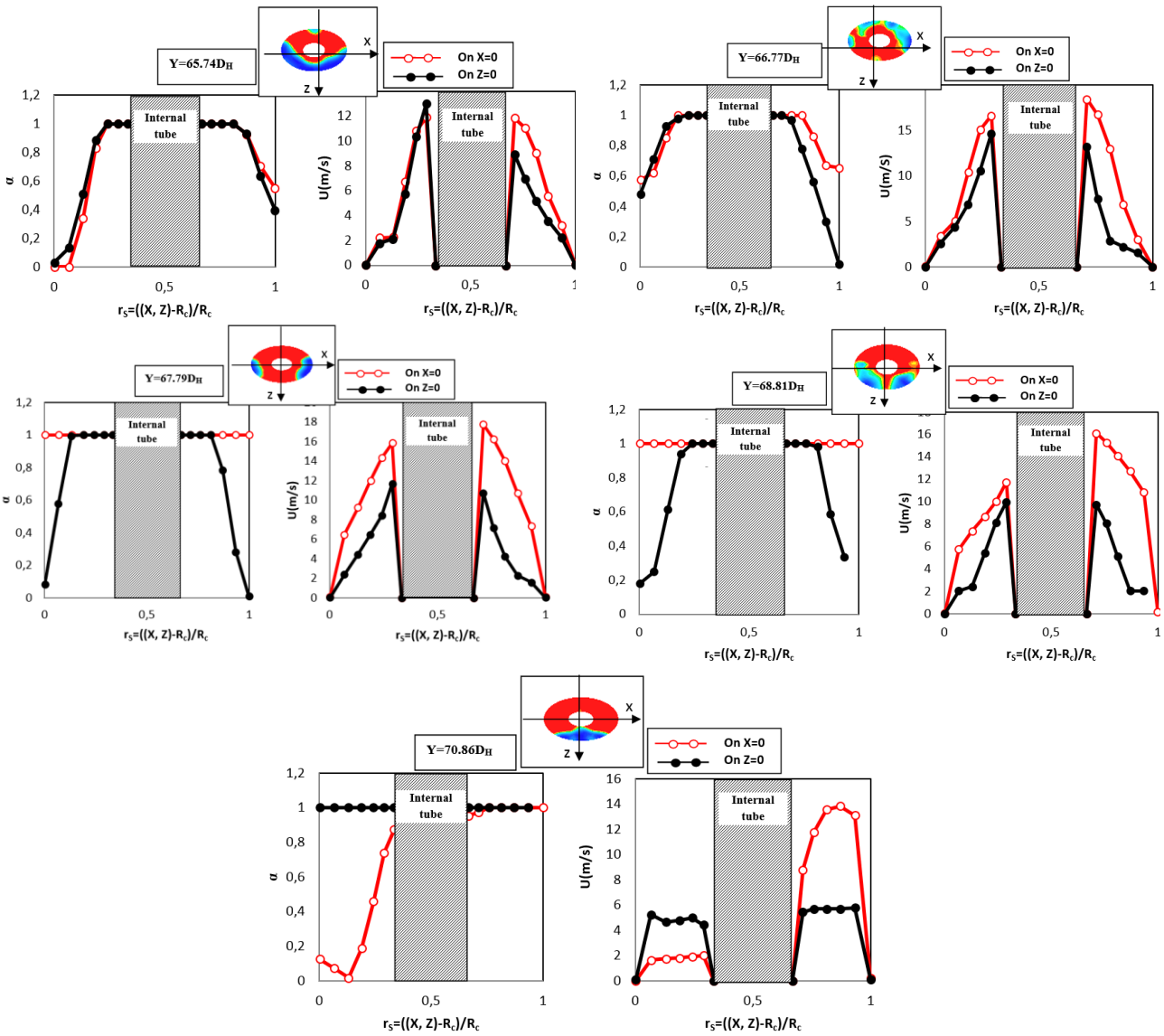

Fig. 19. Evolutions of Air volume fractions (left), and mixture total velocity (right) at different heights: y=65.74D_H, 66.77D_H, 67.79D_H, 68.81D_H, and 70.86D_H for U_g =5 m/s

4. Conclusions

Our numerical study is carried out for the two-phase upward co-flow through vertical concentric annuli. We based in this study on the influence of different air inlet velocity at a fixed water velocity equal to 0.14m/s. The numerical results are presented by curves and fields extracted by numerical computations. The isosurfaces colored by the air volume fractions is illustrated and the contours of the air volume fractions and the instantaneous total mixing velocities are plotted in the horizontal and vertical plans (xoy), (yoz and yoz), respectively. Also, the profiles of the volume fraction of the air and these of the total velocity of the mixture were drawn along the tangent lines on the selected planes and oriented the two axes ox and oz or (x = 0 and z = 0).

The important conclusions drawn from this study are listed in the following.

I. Basic two-phase flow regimes are observed for the proposed velocities. These regimes flow are obtained according to the increase of the air velocity, such as, the bubbles, the slug, the strong coalescence and the annular régimes, they are followed by flow patterns transition.

II. The capability of the VOF numerical model for giving different peak structures of the air volume fractions distribution in the bubble flow has been observed. Similarly, peaks of the average total velocity of the mixture close to the outer tube inner wall increase with the gradual increase in the superficial velocity of the air. For example, in the bubble regime, it was calculated that the average void fraction is 30%, whereas this value was 25% for the numerical calculation and the experimental measurement of Das *et al.,* and others, they are approximately close.

These results are consistent with the experimental investigation of Das *et al.,* [3].

References

[1] Caetano, E. F., O. Shoham, and J. P. Brill. "Upward vertical two-phase flow through an annulus—Part II: Modeling bubble, slug, and annular flow." *Journal of Energy Resources Technology* 114, no. 1 (1992): 14-30.

[2] Caetano, E. F., O. Shoham, and J. P. Brill. "Upward vertical two-phase flow through an annulus—part i: single-phase friction factor, Taylor bubble rise velocity, and flow pattern prediction." *Journal of Energy Resources Technology* 114, no. 1 (1992): 1-13.

[3] Das, G., P. K. Das, N. K. Purohit, and A. K. Mitra. "Rise velocity of a Taylor bubble through concentric annulus." *Chemical engineering science* 53, no. 5 (1998): 977-993.

[4] Das, G., P. K. Das, N. K. Purohit, and A. K. Mitra. "Flow pattern transition during gas liquid upflow through vertical concentric annuli—part I: experimental investigations." *Journal of fluids engineering* 121, no. 4 (1999): 895-901.

[5] Eyo, Edem Nsefik, and Liyun Lao. "Gas-liquid flow regimes in horizontal annulus." *Journal of Petroleum Science and Engineering* 175 (2019): 573-586.

[6] Ibarra, Roberto, and Jan Nossen. "Bubble velocity in horizontal and low-inclination upward slug flow in concentric and fully eccentric annuli." *Chemical Engineering Science* 192 (2018): 774-787.

[7] Movahedi, Hamed, Saeed Shad, and Zahra B. Mokhtari-Hosseini. "Modeling and simulation of barite deposition in an annulus space of a well using CFD." *Journal of Petroleum Science and Engineering* 161 (2018): 476-496.

[8] Julia, J. Enrique, and Takashi Hibiki. "Flow regime transition criteria for two-phase flow in a vertical annulus." *International Journal of Heat and Fluid Flow* 32, no. 5 (2011): 993-1004.

[9] Sorgun, M., R. E. Osgouei, M. E. Ozbayoglu, and A. M. Ozbayoglu. "An experimental and numerical study of two-phase flow in horizontal eccentric annuli." *Energy Sources, Part A: Recovery, Utilization, and Environmental Effects* 35, no. 10 (2013): 891-899.

[10] Hibiki Takashi, Ye Mi, Rong Situ, and Mamoru Ishii. "Interfacial area transport of vertical upward bubbly two-phase flow in an annulus." *International Journal of Heat and Mass Transfer* 46, no. 25 (2003): 4949-4962.

[11] Das, G., P. K. Das, N. K. Purohit, and A. K. Mitra. "Flow pattern transition during gas liquid upflow through vertical concentric annuli—part II: mechanistic models." *Journal of fluids engineering* 121, no. 4 (1999): 902-907.

[12] Hibiki Takashi, Rong Situ, Ye Mi, and Mamoru Ishii. "Local flow measurements of vertical upward bubbly flow in an annulus." *International Journal of Heat and Mass Transfer* 46, no. 8 (2003): 1479-1496.

[13] Sorour, M. M., and M. S. El-Beshbeeshy. "Void fraction and pressure fluctuations of bubbly flow in a vertical annular channel." *Experiments in fluids* 4, no. 3 (1986): 163-170.

[14] Gaither, Orville D., Herald W. Winkler, and C. V. Kirkpatrick. "Single-and two-phase fluid flow in small vertical conduits including annular configurations." *Journal of Petroleum Technology* 15, no. 3 (1963): 309-320.

[15] James, P. W., and P. Hutchinson. "Droplet deposition in an annular geometry." *International Journal of Multiphase Flow* 5, no. 2 (1979): 103-112.

[16] Das, A. K., and P. K. Das. "Modelling bubbly flow and its transitions in vertical annuli using population balance technique." *International Journal of Heat and Fluid Flow* 31, no. 1 (2010): 101-114.

[17] Kelessidis, V. C., and A. E. Dukler. "Modeling flow pattern transitions for upward gas-liquid flow in vertical concentric and eccentric annuli." *International Journal of Multiphase Flow* 15, no. 2 (1989): 173-191.

[18] Sun, X., S. Kuran, and M. Ishii. "Cap bubbly-to-slug flow regime transition in a vertical annulus." *Experiments in fluids* 37, no. 3 (2004): 458-464.

[19] Ozar, B., C. S. Brooks, D. J. Euh, T. Hibiki, and M. Ishii. "Investigation of one-dimensional interfacial area transport for vertical upward air–water two-phase flow in an annular channel at elevated pressures." *Nuclear Engineering and Design* 263 (2013): 362-379.

[20] Zhao Quanbin and Takashi Hibiki. "One-dimensional drift-flux correlation for vertical upward two-phase flow in large size concentric and eccentric annuli." *International Journal of Multiphase Flow* 113 (2019): 33-44.

[21] Situ Rong, Takashi Hibiki, Xiaodong Sun, Ye Mi, and Mamoru Ishii. "Flow structure of subcooled boiling flow in an internally heated annulus." *International Journal of Heat and Mass Transfer* 47, no. 24 (2004): 5351-5364.

[22] Anglart, Henryk. "Progress in understanding and modelling of annular two-phase flows with heat transfer." *Nuclear Engineering and Design* 345 (2019): 166-182.
[23] Hirt, Cyril W., and Billy D. Nichols. "Volume of fluid (VOF) method for the dynamics of free boundaries." *Journal of computational physics* 39, no. 1 (1981): 201-225.
[24] ANSYS Inc., (2016), Guide de l'utilisateur ANSYS FLUENT 17.1, Canonsburg, Pennsylvanie, États-Unis d'Amérique
[25] Ubbink, Onno. "Numerical prediction of two fluid systems with sharp interfaces." PhD thesis, University of London, (1997).
[26] Muzaferija, Samir. "Computation of free surface flows using interface-tracking and interface-capturing methods." *Nonlinear water-wave interaction. Computational Mechanics, Southampton* (1998).
[27] Brackbill, Jeremiah U., Douglas B. Kothe, and Charles Zemach. "A continuum method for modeling surface tension." *Journal of computational physics* 100, no. 2 (1992): 335-354.
[28] Launder, Brian Edward, and Dudley Brian Spalding. "The numerical computation of turbulent flows." *Computer Methods in Applied Mechanics and Engineering* 3 (1974): 269-289.
[29] Shen, Y. M., C. O. Ng, and Y. H. Zheng. "Simulation of wave propagation over a submerged bar using the VOF method with a two-equation k–ε turbulence modeling." *Ocean Engineering* 31, no. 1 (2004): 87-95.
[30] Patankar, Suhas V., and D. Brian Spalding. "A calculation procedure for heat, mass and momentum transfer in three-dimensional parabolic flows." In *Numerical Prediction of Flow, Heat Transfer, Turbulence and Combustion*, pp. 54-73. Pergamon, 1983.